# Automatic Line Segment Registration Using Gaussian Mixture Model and Expectation-Maximization Algorithm

Tengfei Long, Weili Jiao, Guojin He, and Wei Wang

***Abstract*—Line segment registration (LSR) for image pairs is a challenging task but plays an important role in remote sensing and photogrammetry. This paper proposes a line segment registration method using Gaussian Mixture Models (GMMs) and Expectation-Maximization (EM) algorithm. Comparing to the conventional registration methods which consider the local appearance of points or line segments, the proposed method of LSR uses only the spatial relations between the line segments detected from an image pair, and it does not require the corresponding line segments sharing the same start points and end points. Although the proposed method is not confined to the transformation model between the image pair, the affine model, which is a simple and fast registration model and widely used in remote sensing, is taken to verify the proposed method. Various images including aerial images, satellite images and GIS data are used to test the algorithm, and test results show that the method is robust to different conditions, including rotation, noise and illumination. The results of the proposed method are compared with those of other line segment matching methods, and it is shown that the proposed method is superior in matching precision and performs better in less-texture or no-texture case.**

***Index Terms*—Registration, Line Segment, Matching, Gaussian Mixture Model, Expectation Maximization.**

## I. Introduction

Image registration is a basic and crucial step for comparing or integrating the data obtained from different sensors, from different times, or from different viewpoints, and has drawn a lot of attention for decades. The majority of the registration methods consist of the following four steps: feature detection, feature matching, transform model estimation and image transformation [1]. So far, invariant descriptor based methods are widely used in registration due to their invariance to the expected image deformation [2]. SIFT, proposed by David Lowe in 1999 [3], has proven remarkably successful in feature detecting and matching but imposes a heavy computational burden. Several improved descriptors including SURF [4], DAISY [5], BRISK [6], ORB [7] and FREAK [8], have been proposed in the last few years, and some of these descriptors are efficient enough to perform a real time registration. In remote sensing, however, the images are usually obtained from different sensors, different times or different spectral bands, and their intensity and hue may be quite different from each other [9]. The feature descriptors, which depend on the intensity and texture information of the images, may fail to find the repeatable feature points when the images (such as digital maps) lack of rich textures. Moreover, identified points are usually not sufficient and not evenly distributed. In this case, the straight line segments are commonly considered as alternatives or supplements of the points in image registration.

Line segments detected in images are typically more stable than points and are less likely to be affected by clutter and noise, especially in man-made environments [10]–[12]. Many methods [13]–[21] have been proposed to estimate the transformation model using line segments, but the line segment matching step does not perform automatically. In fact, line segment based registration algorithms are generally more difficult than point-based ones for the following three reasons: the parameter space of line segments is nonlinear; a line-to-line correspondence contains less information than a point-to-point one [14]; it is difficult to describe a line segment uniquely compared to a point representation. There are generally two ways to match the detected features: using their spatial relations or various descriptors of features [1].

The intuitive characteristics of line segment features, such as length, orientation, and width are not invariant and therefore they are not apt descriptors for line segment features. Various approaches have been proposed to describe the line segments or to measure the similarity of line segment pairs [8], [22]–[25]. Extending point descriptors that have been proven successful to construct descriptors for line segments [26] may be a proper way to develop robust line segment descriptors. A robust descriptor for line segment matching (MSLD, Mean-Standard deviation Line Descriptor) [27] has been proposed recently using a SIFT-like strategy, and it is already applied to rigid registration of remote sensing images [28]. According to the definition of MSLD descriptor, the gradients distributed in sub-regions around a line segment feature are integrated as the components of the descriptor. However, considering that the corresponding line segments do not necessarily share the same end points, the MSLD descriptor may fail to provide correct similarity between a pair of corresponding line segments. By exploiting rich edge attributes and edge geometric structure information, Zhang et al. [29] use similarity measure to compute the edge attributes and epipolar constraint to reduce the search space, and locally consistent matching is achieved through structural matching with probability relaxation. And recently, Fan et al. [30] explore an affine invariant from

This work was supported by the grant from the National Natural Science Foundation of China (61271013) and the National High Technology Research and Development Program of China (863 Program) (2012BAH27B05).

The authors are with the Institute of Remote Sensing and Digital Earth (RADI), Chinese Academy of Sciences.

Tengfei Long is also with the University of Chinese Academy of Sciences.

Corresponding author: Weili Jiao (E-mail: wljiao@ceode.ac.cn).

two points and one line. They utilize this affine invariant to match *Lines* with known *Point* correspondences (LP). The main drawback of these approaches is the requirement of known epipolar geometry or point correspondences. Besides, their performance in less-textured scenes is limited because of the lack of good point correspondences. Additionally, Wang et al. [31] use *Line Signatures* (LS) to match lines between wide baseline images and Zhang et al. [32] use *Appearance* similarities and *Geometric* (AG) constraints to match straight lines. These methods commonly have a good matching performance. However, when the images are less-textured or no-textured, the similarity measurements become useless, and line matching would fail.

By utilizing the space transformation constraints between two sets of the detected line segments, the line-to-line correspondences can be found without considering the similarity of the line segments. The Modified Iterated Hough Transform (MIHT) [33] is a transformation based registration method for linear feature registration which uses a voting strategy evoked from traditional Hough method to estimate the parameters of a mathematical model relating conjugate entities of two data sets, and it provides an alternative approach for pose estimation (space resection) in photogrammetry and remote sensing [34]–[37]. However, several defects of MIHT limit its application in image registration: the Hough-like voting strategy makes the algorithm time consuming and noise sensitive; the algorithm is not proven to converge to an optimized estimator; the correlations among the transformation parameters may cause the algorithm failed because its parameters are estimated separately during each iteration. Another line segment registration approach based on SoftPOSIT [10] is used to determine pose and correspondence simultaneously [38], but the convergence is not guaranteed in the presence of outliers [39].

In contrast to line segment registration, the point registration based on transformation has been extensively studied during the last few years, and various methods are proposed, which can be roughly divided into three categories: the Iterative Closest Point (ICP methods) [40]–[42] , soft assignment methods [43], [44], and probabilistic methods [39], [45]–[48]. Although efficient versions of ICP are attractive for their efficiency, they are particularly sensitive both to initialization and the choice of a threshold needed to accept or to reject a match. For the soft assignment methods, the nearest point strategy of ICP is replaced by a continuous optimizing framework and therefore they are more robust. However, when outliers are involved, soft assignment algorithms do not ensure convergence. Probabilistic point registration generally uses Gaussian Mixture Models (GMMs) [49] and Expectation-Maximization (EM) algorithm [50], and performs better than conventional ICP and soft assignment methods, especially in the presence of noise and outliers. This paper proposes a line segment based automatic image registration method using GMMs with equal isotropic covariance and EM algorithm. This method provides a probabilistic approach to line segment registration (LSR), which is and most closely related to the point registration method introduced in the previous works performed by Myronenko and Song [48] and Horaud et al. [39]. In short, the probabilistic point registration method is extended for line segments, and meanwhile two improvements have been made in this paper: (1) Equal isotropic covariance is proposed to substitute the covariance matrix used in [39] to overcome the additional computing and singularity of inverse. (2) Since the prior of outlier is difficult to determine when the registration problem is cast in the EM framework, a reasonable assumption making the prior a constant is provided instead of being given manually. Moreover, the proposed approach does not require the corresponding line segments sharing the same start points and end points.

The remainder of this paper is organized as follows: In Section II, a framework for line segment registration is proposed. Section III and Section IV show some details of the registration method. In Section III, the representation and distance measurement of line segments are discussed. In Section IV, the transformation model for line segment is discussed, and a fast registration using affine transformation model is additionally provided. In Section V, several line segment registration tests are carried out using aerial images, satellite images and GIS data. Section VI concludes with some discussions.

## II. The EM framework for line segment registration

Commonly speaking, image registration with corresponding observed data is a maximum likelihood problem, which can be solved directly by means of parametric estimation. However, when the correspondences are unknown, various factors, including an unknown transformation, noise, outliers and missing features, make the image registration intractable. Due to the uncertainty of the correspondences, in this study, the registration problem is considered as a probabilistic Gaussian Mixture Models (GMMs), which is a parametric probability density function represented as a weighted sum of Gaussian component densities. The line segments in the slave set represent the GMM centroids, while those in the master set represent the observed data. The correspondences between the line segments are the missing data and are treated as hidden variables. In this sense, the estimation of the registration parameters is equivalent to finding the maximum likelihood of the GMM with auxiliary hidden variables.

### A. Mathematical Notations and Methodology

Throughout this paper, two sets of line segments from two images are considered, and the following notations will be used:

- $\mathbf{I}, \mathbf{I}'$—the slave image and the master image,
- $N, M$—number of line segments in the slave line segment set and the master line segment set,
- $\mathbf{X} = \{\mathbf{x}_1, \mathbf{x}_2, \ldots, \mathbf{x}_N\}$—the slave line segment set (the GMM centroids),
- $\mathbf{Y} = \{\mathbf{y}_1, \mathbf{y}_2, \ldots, \mathbf{y}_M\}$—the master line segment set (the observations),
- $\mathcal{T}(\mathbf{x}, \boldsymbol{\Theta})$—transformation applied to $\mathbf{x}$, where $\boldsymbol{\Theta}$ is a set of the transformation parameters,
- $\|\mathbf{x}, \mathbf{y}\|$—the distance from line segment $\mathbf{x}$ to line segment $\mathbf{y}$ ,

- $\mathbf{P} = \{p_{mn}\}_{1\leq m\leq M, 1\leq n\leq N+1}$—the corresponding matrix, consisting with the hidden variables of the GMM. $p_{mn}$is the posterior probability of that observation $m$ belongs to inlier centroids $n$ when $n \leq N$, while $p_{m(N+1)}$ means the observation $m$ belongs to the outlier cluster,
- $|C|$—the number of the elements of a set $C$.

For the line segment registration problem, the observation log-likelihood function is:

$$\mathcal{L}(\mathbf{\Theta}) = \ln \prod_{m=1}^{M} P(\mathbf{y}_m) \tag{1}$$

where $P(\mathbf{y}_m)$ is the marginal distribution of an observation $m$ in the GMM, and $\mathbf{\Theta}$ is a set of the transformation parameters.

Due to the unknown correspondences between the line segments, it is tough to maximize the function $\mathcal{L}$ directly. So Expectation-Maximization (EM) algorithm is brought in to find the maximum-likelihood estimate of this incomplete-data problem. EM is an iterative method, whose idea is first to guess the values of parameters and then use the Bayes' theorem to compute a posterior probability distributions of mixture components (E-step), and the new parameter values are then found by maximizing the expectation of a complete log-likelihood function (M-step). The E-steps and the M-steps alternately iterate until the convergence conditions are met, and EM algorithm have been proven to converge to a local maximum. The framework for line segment registration is proposed in the following.

### B. Initialization

To begin with, the initial value of the transformation parameter set $\mathbf{\Theta}$ is given as $\mathbf{\Theta}^{(1)}$. Then during the $k_{th}(k \geq 1)$ iteration, the posterior probabilities $p_{mn}^{(k)}$ of GMM components are calculated in the E-step, and a new value of the transformation parameter set $\mathbf{\Theta}^{(k+1)}$, which will be involved in the next iteration, is estimated in the M-step. Now consider the $k_{th}$ iteration of the algorithm, and an estimation value of $\mathbf{\Theta}$ is denoted by $\mathbf{\Theta}^{(k)}$.

### C. The E-step

Denote the prior of GMM centroid $n$ as $P(n)$ for $\forall n, 1 \leq n \leq N$, and the prior of outlier cluster as $P(N+1)$, and then $\sum_{n=1}^{N+1} P(n) = 1$. Then according to the law of total probability, the marginal distribution of an observation $m$ in log-likelihood function (1) can be calculated as:

$$P(\mathbf{y}_m) = \sum_{n=1}^{N+1} P(n)P(\mathbf{y}_m|n) \tag{2}$$

where $P(\mathbf{y}_m|n)$ is the likelihood of an observation $m$ belonging to a centroid $n$ or outlier cluster.

The likelihood of an observation $m$ belonging to an inlier centroid $n$ $(1 \leq n \leq N)$ is drawn from a Gaussian distribution with mean $\mathcal{T}(\mathbf{x}_n, \mathbf{\Theta}^{(k)})$ and equal isotropic covariance $(\sigma^{(k)})^2$:

$$P(\mathbf{y}_m|n) = \frac{1}{2\pi(\sigma^{(k)})^2} \exp(-\frac{\|\mathcal{T}(\mathbf{x}_n, \mathbf{\Theta}^{(k)}), \mathbf{y}_m\|^2}{2(\sigma^{(k)})^2}) \tag{3}$$

The likelihood of an observation $m$ belonging to outlier cluster is a uniform distribution over the volume $V$ of the working space:

$$P(\mathbf{y}_m|N+1) = \frac{1}{V} \tag{4}$$

In the working space, an inlier centroid $n$ is denoted by a small sphere (or a small circle in two dimension case) $s_n$ with radius $r$ centered at centroid: $\mathcal{T}(\mathbf{x}_n, \mathbf{\Theta}^{(k)})$, whose volume is $v = \pi r^2$. The total volume of all $N$ inlier centroids is $v_{in} = v(\bigcup_{n=1}^{N} s_n) \leq v \cdot N$, where $v(\bigcup_{n=1}^{N} s_n)$ is volume of the union of the $N$ small spheres. Then the volume of outlier cluster is $v_{out} = V - v_{in}$.

According to the volumes of the GMM centroids, the priors are given as follows:

$$P(n) = \begin{cases} p_{in} = \frac{v_{in}}{V}, & \text{if } 1 \leq n \leq N \\ p_{out} = \frac{V - v_{in}}{V}, & \text{if } n = N+1 \end{cases} \tag{5}$$

Using Bayes' rule, the posterior probability $p_{mn}$ of that observation $m$ belongs to inlier centroids $n$ or outlier cluster can be derived:

$$p_{mn} = P(n|\mathbf{y}_m) = \frac{P(n)P(\mathbf{y}_m|n)}{P(\mathbf{y}_m)} \tag{6}$$

where $P(n)$, $P(\mathbf{y}_m|n)$ and $P(\mathbf{y}_m)$ come from equation (2), (3), (4) and (5). Then for $\forall n, 1 \leq n \leq N$:

$$p_{mn}^{(k)} = \frac{\frac{1}{2\pi(\sigma^{(k)})^2} \exp(-\frac{\|\mathcal{T}(\mathbf{x}_n, \mathbf{\Theta}^{(k)}), \mathbf{y}_m\|^2}{2(\sigma^{(k)})^2}) \frac{v}{V}}{\frac{V - v_{in}}{V^2} + \sum_{q=1}^{N} \left( \frac{v}{2\pi V(\sigma^{(k)})^2} \exp(-\frac{\|\mathcal{T}(\mathbf{x}_q, \mathbf{\Theta}^{(k)}), \mathbf{y}_m\|^2}{2(\sigma^{(k)})^2}) \right)} \tag{7}$$

Additionally, by assuming that $v_{in} \leq v \cdot N \ll V$, formula (7) can be simplified as:

$$p_{mn}^{(k)} = \frac{\exp(-\frac{\|\mathcal{T}(\mathbf{x}_n, \mathbf{\Theta}^{(k)}), \mathbf{y}_m\|^2}{2(\sigma^{(k)})^2})}{c + \sum_{q=1}^{N} \left( \exp(-\frac{\|\mathcal{T}(\mathbf{x}_q, \mathbf{\Theta}^{(k)}), \mathbf{y}_m\|^2}{2(\sigma^{(k)})^2}) \right)} \tag{8}$$

where $c = (2\pi(\sigma^{(k)})^2)/(\pi r^2) = 2(\sigma^{(k)}/r)^2$. Here $r = 3\sigma^{(k)}$, indicating that about 99.7% of the data [51] around a GMM centroid are involved in the small sphere. In this case, $c$ is a constant and $c = 2/9$.

The posterior probability of outlier is given by:

$$p_{m(N+1)}^{(k)} = 1 - \sum_{n=1}^{N} p_{mn}^{(k)} \tag{9}$$

Up to now, the E-step of EM algorithm is finished, and the expectation of the observation log-likelihood function (1) can be derived as:

$$E(\mathcal{L}(\mathbf{\Theta})) = \sum_{m=1}^{M} \sum_{n=1}^{N+1} P^{(k)}(n|\mathbf{y}_m) \ln P(n)P(\mathbf{y}_m|n) \tag{10}$$

### D. The M-step

The next is the M-step of the EM algorithm. By ignoring the constants independent of $\Theta$ and reversing the sign, the objective function (11) can be derived from formula (10):

$$Q(\mathbf{\Theta}) = \frac{1}{2(\sigma^{(k)})^2} \sum_{m=1}^{M} \sum_{n=1}^{N} p_{mn}^{(k)} \|\mathcal{T}(\mathbf{x}_n, \mathbf{\Theta}), \mathbf{y}_m\|^2 \quad (11)$$

Admittedly, maximizing function (10) is equivalent to minimizing function (11), and $\mathbf{\Theta}^{(k+1)}$, which minimizes function (11), will be used to calculate the new posterior probability $p_{mn}^{(k+1)}$ in the next iteration.

The new transformation parameter set $\mathbf{\Theta}^{(k+1)}$ results in a new isotropic covariance:

$$(\sigma^{(k+1)})^2 = \frac{\sum_{m=1}^{M} \sum_{n=1}^{N} p_{mn}^{(k)} \|\mathcal{T}(\mathbf{x}_n, \mathbf{\Theta}^{(k+1)}), \mathbf{y}_m\|^2}{\sum_{m=1}^{M} \sum_{n=1}^{N} p_{mn}^{(k)}} \quad (12)$$

### E. Termination conditions

Three termination conditions for the EM based registration algorithm are provided. They are on the variation of parameter set $\mathbf{\Theta}$, the covariance $\sigma^2$ and the variation of covariance $\sigma^2$, respectively. If any of the following conditions is satisfied, the algorithm will be terminated:

$$\begin{aligned} &(1) \quad \|\mathbf{\Theta}^{(k)} - \mathbf{\Theta}^{(k-1)}\|_{L2} < \epsilon_1; \\ &(2) \quad (\sigma^{(k)})^2 < \epsilon_2; \\ &(3) \quad |(\sigma^{(k)})^2 - (\sigma^{(k-1)})^2| < \epsilon_3. \end{aligned} \quad (13)$$

where $\|\bullet\|_{L2}$ is the $\ell^2$-norm, and $\epsilon_1$, $\epsilon_2$ and $\epsilon_3$ are the threshold values. Empirically, $\epsilon_1 = 10^{-6}$, $\epsilon_2 = 1.0$, and $\epsilon_3 = 0.1$.

### F. Assignment and outlier exclusion

When the iterations of EM algorithm finish, the final corresponding matrix $\mathbf{P} = \{p_{mn}\}$ is obtained. Then the next job is to assign each observation to a centroid or outlier cluster, and the following rule [39] is used to get the assignments:

$$z_m = \arg\max_n p_{mn} \quad (14)$$

where $z_m$ indicates that the observation $m$ is corresponding to the centroid $n$ (if $n \leq N$), or is an outlier (if $n = N + 1$).

Finally, to make the matching result more reliable, an enhanced version of RANSAC [52] is used to get rid of the outliers produced by mismatching. Then the final matching results (the control line segments), are yielded.

### G. Algorithm summary

Up to now, the framework of registration using EM algorithm is established. The implementation of the method will be introduced in details in section III and section IV. Here, the framework of EM based *line segment registration* (LSR) algorithm is summarized in Algorithm 1.

**Algorithm 1:** Line Segment Registration (LSR)

**Initialization**:

a. Choose the initial value $\mathbf{\Theta}^1$ for the transformation parameter set;

b. Set the thresholds $\epsilon_1 = 10^{-6}$, $\epsilon_2 = 1$ and $\epsilon_3 = 10^{-1}$;

c. Set the initial posterior probabilities as $p_{mn}^{(0)} = \frac{1}{N+1}$;

d. Evaluate the initial covariance $(\sigma^{(1)})^2$ from equation (12);

e. Set $k = 1$ and go to **E-Step**;

**E-Step**:

a. Calculate the posterior probabilities $p_{mn}^{(k)}$ from equation (8) and (9), using the current parameters $\mathbf{\Theta}^{(k)}$ and $(\sigma^{(k)})^2$;

**M-Step**:

a. Find the minimizer ($\mathbf{\Theta}^{(k+1)}$) of the objective function equation (11), using current posterior probabilities $p_{mn}^{(k)}$ and covariance $(\sigma^{(k)})^2$;

b. Update the isotropic covariance as $(\sigma^{(k+1)})^2$ from equation (12), using current parameters $\mathbf{\Theta}^{(k+1)}$ and posterior probabilities $p_{mn}^{(k)}$;

**Check termination conditions**:

a. If any of the three conditions in equation (13) is satisfied, go to **Assignment** step; Else, return to **E-Step** with parameters $\mathbf{\Theta}^{(k+1)}$ and covariance $(\sigma^{(k+1)})^2$;

**Assignment**:

a. Assign each observation to a centroid or an outlier according to formula (14), and get the matched line segments;

**Outlier exclusion**:

a. Get rid of the unreliable matched line segments using RANSAC method, and obtain the final matching result;

**Output**: matched line segments

## III. The Distance Measurement of Line Segments

### A. Representation of line segment

In this section, the distance between line segments, which is the basic measurement in the line segment registration problem, is discussed in detail. Only the case of a 2D line segment is considered here, since the 3D case is more complicated. As a line segment feature in an image is a segment with two end points, the line segment can be directly represented by the two end points, i.e. $(x_1, y_1, x_2, y_2)^\top$. All the line segments in the image can be expressed in this form even if they are vertical or horizontal, and it is convenient to get the coordinates of the end points. However, this form does not explicitly tell the characteristics of a line segment, such as slope angle and intercept. So another mathematical form of a line segment is considered:

$$\rho = -x \sin\theta + y \cos\theta \quad (15)$$

where $(x, y)$ is a point on the line segment, while $\rho$ and $\theta$ are the parameters.

One can easily tell the slope angle and intercept of a line segment from this form but not the end points. To take the

advantages of both mathematical forms, six parameters are used to represent a 2D line segment:

$$\overline{P_1P_2} := (x_1, y_1, x_2, y_2, \rho, \theta)^\top \tag{16}$$

where $(x_1, y_1)$ and $(x_2, y_2)$ is the coordinates of point $P_1$ and $P_2$.

Obviously, the six parameters are not independent due to the following constraints:

$$\begin{cases} \rho = -x_1 \sin\theta + y_1 \cos\theta \\ \rho = -x_2 \sin\theta + y_2 \cos\theta \end{cases} \tag{17}$$

One can derive $\rho$ and $\theta$ from $(x_1, y_1)$ and $(x_2, y_2)$ according to formula (17). In this study, line segments are represented using form (16).

### B. Distance measurement of line segment

The distance from a point $(x, y)$ to a line segment $(x_1, y_1, x_2, y_2, \rho, \theta)^\top$ is:

$$| - x \sin\theta + y \cos\theta - \rho|$$

Considering two line segments $\mathbf{x}(x_1, y_1, x_2, y_2, \rho, \theta)^\top$ and $\mathbf{y}(x_1', y_1', x_2', y_2', \rho', \theta')^\top$, the distances from the two end points of $\mathbf{y}$ to segment $\mathbf{x}$ are:

$$\begin{cases} d_1 = |-x_1' \sin\theta + y_1' \cos\theta - \rho| \\ d_2 = |-x_2' \sin\theta + y_2' \cos\theta - \rho| \end{cases} \tag{18}$$

Here the superiority of this form (16) is shown – the distance formula is linear for $x_1'$, $y_1'$, $x_2'$ and $y_2'$.

Similarly, distances from the two end points of $\mathbf{x}$ to segment $\mathbf{y}$ can also be calculated, and they are denoted as $d_1'$ and $d_2'$, respectively.

Two definitions of distance between two line segments are given.

1) The distance from segment $\mathbf{y}$ to segment $\mathbf{x}$ is defined as:

$$\|\mathbf{y}, \mathbf{x}\|_1 = \sqrt{d_1^2 + d_2^2} \tag{19}$$

where $d_1$ and $d_2$ come from formula (18), and they are the two components of the distance vector.

2) The distance between two segments $\mathbf{x}$ and $\mathbf{y}$ is defined as:

$$\|\mathbf{x}, \mathbf{y}\|_2 = \|\mathbf{y}, \mathbf{x}\|_2 = \sqrt{\|\mathbf{x}, \mathbf{y}\|_1^2 + \|\mathbf{y}, \mathbf{x}\|_1^2} \tag{20}$$

where $\|\mathbf{x}, \mathbf{y}\|_1$ and $\|\mathbf{y}, \mathbf{x}\|_1$ come from formula (19), and they are the two components of the distance vector. Explicitly, $\|\mathbf{x}, \mathbf{y}\|_2 = \sqrt{d_1^2 + d_2^2 + d_1'^2 + d_2'^2}$.

Figure 1 shows the distance of $d_1$, $d_2$, $d_1'$, and $d_2'$.

Both $\|\bullet\|_1$ and $\|\bullet\|_2$ can be used as the measurement of distance between two line segments. $\|\bullet\|_1$ is simpler than $\|\bullet\|_2$ but not as constraining as it.

## IV. The Transformation Model

### A. General transformation model

$\mathcal{T}(\mathbf{x}, \mathbf{\Theta})$ is a generic transformation of line segment, which can be specified in various situations. Substantially, the transformation of a line segment is the transformation of end points of the segment, and the transformation can be given by

$$\begin{cases} x' = f_x(X, Y, Z, \mathbf{\Theta}) \\ y' = f_y(X, Y, Z, \mathbf{\Theta}) \end{cases} \tag{21}$$

or

$$\begin{cases} x' = f_x(x, y, \mathbf{\Theta}) \\ y' = f_y(x, y, \mathbf{\Theta}) \end{cases} \tag{22}$$

Formula (21) is a 3D-2D transformation and formula (22) is a 2D-2D transformation. The 3D-2D transformation model is extensively used to rectify images in photogrammetry and remote sensing, including collinear equation, direct linear transformation model and rational polynomial model. In the authors' previous work [53], geometric rectification using line segment features was discussed in detail, and the method can be used to minimize the objective function (11). Generally speaking, the transformation model of a line segment is nonlinear, and the minimization of formula (11) can be taken as nonlinear weighted least squares whose analytic solution is unavailable. Then Levenberg-Marquardt optimization algorithm with numerical Jacobian matrix [54] is a proper approach to find the minimizing of the objective function. Although the proposed approach could potentially be utilized to general transformation model cases, we do not provide the experiment results of the general cases in the paper. Instead, we take the affine transformation model as an example in IV-B to deduce a fast registration.

### B. Fast registration using affine transformation

In this subsection, affine transformation model is discussed in detail. Affine transformation model is a simple but efficacious approximation of the geometric model of imagery captured by high resolution satellite imaging systems with narrow angular field of view and long focus [55]. To be worth mentioning, in the bias-compensated RFM (Rational Function Model) [56], which is widely used in high resolution satellite images, the biases are usually modeled as affine. A linear solution, which promises to accelerate the registration process, is provided for

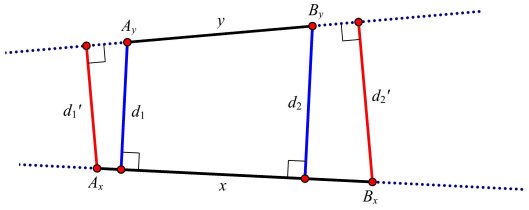


Fig. 1. The distance of $d_1$, $d_2$, $d_1'$, and $d_2'$ of line segment $\mathbf{x}$ and $\mathbf{y}$. $A_x$ and $B_x$ are the two end points of line segment $\mathbf{x}$, and $A_y$ and $B_y$ are the two end points of line segment $\mathbf{y}$. $d_1$ is the distance from point $A_y$ to line segment $\mathbf{x}$, $d_2$ is the distance from point $B_y$ to line segment $\mathbf{x}$, $d_1'$ is the distance from point $A_x$ to line segment $\mathbf{y}$, and $d_2'$ is the distance from point $B_x$ to line segment $\mathbf{y}$.

the line segment registration based on affine transformation model in this subsection. Taking the affine transformation model as example:

$$\begin{cases} x' = a_0 + a_1 X + a_2 Y \\ y' = b_0 + b_1 X + b_2 Y \end{cases} \tag{23}$$

where $(X, Y)$ is the coordinates of the point before transformation, $(x', y')$ is the coordinates of the point after transformation, and $a_0 \sim b_2$ are the affine transformation parameters.

In order to minimize the objective function (11), the term $\mathcal{T}(\mathbf{x}_n, \mathbf{\Theta})$ should be estimated firstly. Here the transformation parameter set $\mathbf{\Theta} = (a_0, a_1, a_2, b_0, b_1, b_2)^\top$, and the 2D line segment $\mathbf{x}_n$ is denoted as $(X_1^n, Y_1^n, X_2^n, Y_2^n)^\top$, then,

$$\mathbf{x}'_n = \mathcal{T}(\mathbf{x}_n, \mathbf{\Theta}) = \begin{pmatrix} a_0 + a_1 X_1^n + a_2 Y_1^n \\ b_0 + b_1 X_1^n + b_2 Y_1^n \\ a_0 + a_1 X_2^n + a_2 Y_2^n \\ b_0 + b_1 X_2^n + b_2 Y_2^n \\ \rho'^n \\ \theta'^n \end{pmatrix} \tag{24}$$

Denote $\mathbf{y}_m = (x_1^m, y_1^m, x_2^m, y_2^m, \rho^m, \theta^m)^\top$, then,

$$\|\mathcal{T}(\mathbf{x}_n, \mathbf{\Theta}), \mathbf{y}_m\| = \sqrt{d_1^2 + d_2^2} \tag{25}$$

where

$$\begin{cases} d_1 = | -(a_0 + a_1 X_1^n + a_2 Y_1^n)\sin\theta^m \\ \quad + (b_0 + b_1 X_1^n + b_2 Y_1^n)\cos\theta^m - \rho^m | \\ d_2 = | -(a_0 + a_1 X_2^n + a_2 Y_2^n)\sin\theta^m \\ \quad + (b_0 + b_1 X_2^n + b_2 Y_2^n)\cos\theta^m - \rho^m | \end{cases} \tag{26}$$

Here $\|\bullet\|_1$ is used as the measurement of distance. Then two linear error equations on parameter set $\mathbf{\Theta} = (a_0, a_1, a_2, b_0, b_1, b_2)^\top$ can be derived from equation (26) as:

$$\begin{pmatrix} -v_1 \\ -v_2 \end{pmatrix} = \begin{pmatrix} -\sin\theta^m & -\sin\theta^m \\ -X_1^n \sin\theta^m & -X_2^n \sin\theta^m \\ -Y_1^n \sin\theta^m & -Y_2^n \sin\theta^m \\ \cos\theta^m & \cos\theta^m \\ X_1^n \cos\theta^m & X_2^n \cos\theta^m \\ Y_1^n \cos\theta^m & Y_2^n \cos\theta^m \end{pmatrix}^\top \begin{pmatrix} a_0 \\ a_1 \\ a_2 \\ b_0 \\ b_1 \\ b_2 \end{pmatrix} - \begin{pmatrix} \rho^m \\ \rho^m \end{pmatrix} \tag{27}$$

The minimization of the objective function (11) is equivalent to weighted linear least squares, whose weights are $p_{mn}$ and error equations are (27), and the minimized $\hat{\mathbf{\Theta}}$ can be directly calculated without iteration. However, considering that $\|\bullet\|_1$ is not as constraining as $\|\bullet\|_2$, $\|\bullet\|_1$ is just in the M-step, whereas $\|\bullet\|_2$ is used in the E-step.

Although affine model is widely used in photogrammetry and remote sensing, it does not always approximate the image distortion well, and then other specific geometric models can be applied as IV-A introduces. However, in the experiments conducted in V, the test images are all small patches, and the distortion of the image can be approximated with affine model in the range of a remote sensing image patch.

## V. Experiments and Analysis

In this section, we carry out several groups of experiments to show the effects of the proposed line segment registration method, and the experimental data involve aerial stereo images, satellite images and GIS data. In all the experiments described in this section, the line segments are automatically detected using the LSD (Line Segment Detector) [57], which is faster and more robust than the commonly used Hough Transform method. Additionally, three line segment matching methods, including the line matching using Appearance similarities and Geometric constraints(AG) [32], the Line matching leveraged by Point correspondences (LP) [30] and the Line Signature(LS) [31], are utilized on the same testing data, and provide some comparative results. The implementations of LS, LP and AG are supplied by their authors, and the parameters are chosen as recommended in their original papers. All the experiments are performed on a 2.5GHz Intel(R) Core 2 processor with 2 GB of RAM.

The affine transformation model is utilized in all the following tests, and the same parameters are applied. The scale parameter of LSD is 0.7, and the initial affine model parameters are $\mathbf{\Theta} = (0, 1, 0, 0, 0, 1)^\top$, which indicates that no geometric transformation is made in the initial state.

As the distance formula (19) is not symmetrical ($|\mathbf{y}, \mathbf{x}\|_1 \not\equiv |\mathbf{x}, \mathbf{y}\|_1$), the sequence of the master image and the slave image may slightly affect the quantity of the matched line segments. But commonly, this effect can be omitted. In the experiments, our selection is based on the principle that the images with higher spatial resolution and georeference accuracy are selected as master images.

### A. Simulated experiments

*1) Experiments under rotation, noise and illumination changes:* In this subsection, an aerial image patch is utilized as the master image, and four simulated image patches are obtained by applying manual processing on the master image. Figure 2 shows the processed images. Figure 2a is obtained by rotating the master image patch for 20°. Figure 2b is obtained by adding Gaussian noise with zero mean and standard deviation of 20 to the rotated image patch. Figure 2c is obtained by changing the contrast and brightness of the rotated image patch using equation (28), where $\alpha = 1/3$ and $\beta = -20$.

$$g(i, j) = \alpha \cdot f(i, j) + \beta \tag{28}$$

where $i$ and $j$ indicate that the pixel is located in the $i_{th}$ row and $j_{th}$ column, $f(i, j)$ is the source image pixels, $g(i, j)$ is the output image pixels, $\alpha$ is the contrast parameter and $\beta$ is the brightness parameter.

Table I lists the matching results and the time consuming of the four tests.

The results in Figure 2 and Table I show the robustness of the proposed method under different conditions, including rotation, noises and illumination.

According to Table I, we can see that:

- More than two hundreds of corresponding line segments are founded within tens of seconds, and after outlier elimination by RANSAC approach, the correct ratio of the line segment matches is better than 99.5%.

TABLE I
LINE SEGMENT MATCHING RESULTS OF THE SIMULATED EXPERIMENTS.

| Test | Detected line segments | | Matched line segments | | | | | Time (s) |
|---|---|---|---|---|---|---|---|---|
| | Master | Slave | All | CR (%) | RANSAC | False | CR (%) | |
| Rotation | 563 | 635 | 393 | 97.7 | 349 | 1 | 99.7 | 26.962 |
| Noise | 563 | 359 | 279 | 98.8 | 222 | 1 | 99.5 | 28.018 |
| Dim | 563 | 518 | 305 | 99.3 | 299 | 0 | 100 | 25.534 |

Note: CR = Correct Ratio

(a) (b) (c)

Fig. 2. Manually processed images: (a) The rotated image. (b) The image added noises. (c) The dimmed image.

- Although the sizes of the image patches in the four tests are the same, the consumed times for line segment matching are different. There are mainly two factors affect the time consuming. Firstly, the quantities of the detected line segments, which are utilized as candidates of corresponding line segments, indicate the search space of the matching algorithm. Secondly, the ratio of real corresponding line segments out of all the detected line segments affects the consumed times. In other words, too much outliers involved in the observation data can make the correct estimation difficult. Whereas the matching results can be improved if specific parameters are utilized for different tests, we choose a consistent scale parameter for the LSD algorithm in the four groups of tests to show the robustness of the proposed method.

*2) Performance under different conditions of rotation, noise and illumination:* In this subsection, the master image in V-A1 is used to generate three groups of slave images:

(i) The first group of slave images are obtained by rotating the master image for different degrees, which are selected from the range of $[0°, 350°]$ with an increment of $10°$.
(ii) The second group of slave images are obtained by adding different Gaussian noise to the rotated image in V-A1. The means of the Gaussian noise are zeros, and the standard deviations of the Gaussian noise are selected from the range of $[4, 100]$ with an increment of 2.
(iii) The third group of slave images are obtained by changing the contrast and brightness of the rotated image in V-A1 using equation (28). Four values (1,1/2,1/3,1/4) are selected for the contrast parameter $\alpha$, and the brightness parameter $\beta$ is selected from the range of $[-200, 200]$ with an increment of 20.

For the last two groups of slave images, the initial affine model parameter set is $\mathbf{\Theta} = (0, 1, 0, 0, 0, 1)^\top$. But for the first group of slave images, four initial angles ($0°$, $90°$, $180°$ and $270°$) are used to calculate four initial affine models, which are applied to all of these slave images, respectively. Figure 3 shows the performance curves of the three group of tests, including the correctly matched line segments and the correct ratios.

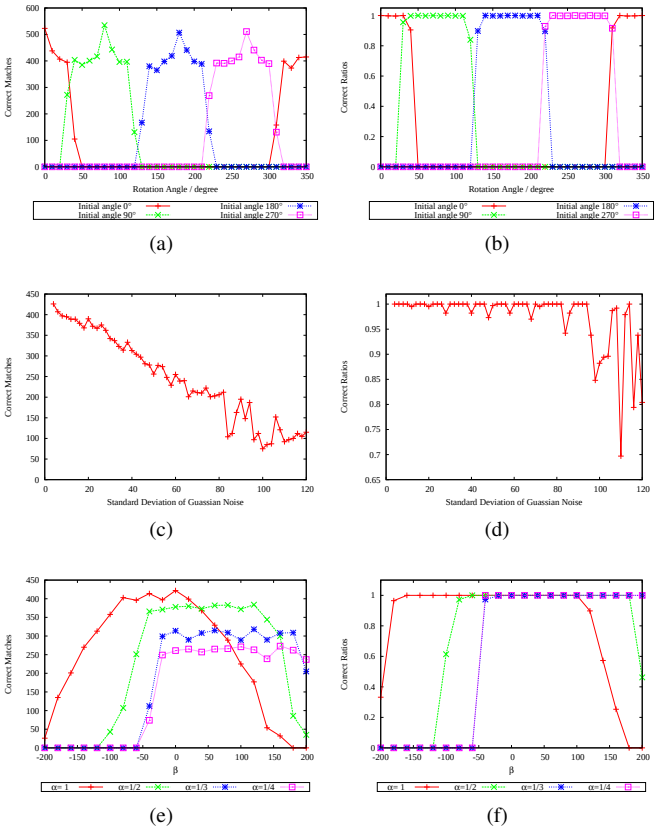


Fig. 3. Performance curves for our method in different conditions: (a) The correct matches under rotations. (b) The correct ratios under rotations. (c) The correct matches under noise. (d) The correct ratios under noise. (e) The correct matches under contrast and brightness changes. (f) The correct ratios under contrast and brightness changes.

We can see from Figure 3 that:

- The performance of our approach is related to the initial transformation parameter set in the rotation tests. When the true rotation angle is within the range of $[-40°, +40°]$ from the initial angle, our approach is robust to find matched line segments with high correct ratios (better than $90\%$). However, when the difference between the true angle and the initial angle is greater than $50°$, our approach may fail. Luckily, as the remote sensing images can be roughly corrected according to their orbit information,

the tolerance of $\pm 40^\circ$ is commonly robust enough. We can also increase the robustness by starting from different initial transformation models, but that will take more time to perform the registration. Moreover, PCA algorithm can be applied to guess the initial transformation model [58]. However, in this work, we considered a fixed initial transformation model for all images, and the estimation of the different initial transformation models for better image matching and registration will be performed in a future work.

- As the increase of the standard deviation of the added Gaussian noise, the quantity of the matched line segments declines gradually, but the correct ratio of the matched line segments does not evidently decrease when the standard deviation is less than 80. The high correct ratios (better than $95\%$) indicate that the matching results are reliable although less corresponding line segments are found. As a matter of fact, much less line segments are detected when Gaussian noise with great standard deviation is added to the image, and the quantity of matched line segments will accordingly decline. However, when the standard deviation of the added Gaussian noise is greater than 80, the matching result becomes instable. As the repeatable line segments are not available in the image with too much noise, the matching algorithm may fail to find corresponding line segments.
- For the original contrast ($\alpha = 1$), the matching results are reliable when the brightness change varies from $-180$ to $+100$, which indicates the breakdown limits of the matching approach. However, the breakdown limits are related to the original contrast and brightness of the image. When the contrast of the image decreases by $1/2$ ($\alpha = 1/2$), the reliable range becomes $[-80, 180]$; and when the contrast of the image decreases by $1/3$ and $1/4$ ($\alpha = 1/3$ and $\alpha = 1/4$), the reliable range is $[-40, 200]$. According to Figure 3e, the number of correctly matched line segments generally declines as the contrast decreases. The reason is that less line segments can be distinguished from an image of low contrast than from one of high contrast. Similar phenomenon happen in the cases around the breakdown limits, as many details of the image are lost when the image becomes too dark or too bright.
- Figure 3 shows the breakdown limits of the proposed approach for rotation, noise, contrast and brightness. Generally speaking, the quantity of correctly matched line segments gradually declines as the conditions change, while the correct ratio does not decline accordingly until the breakdown limits reach. In this sense, although the change in conditions affects the matched line segments, the matched results are reliable. As a result, we can conclude that the proposed approach is found to be robust to rotation, noise, contrast and brightness.

### B. Experiments using real images

Three groups of tests (Test 1, Test 2 and Test 3) are carried out in this subsection, and the proposed method is applied to perform the registration. In each group of test, the estimated affine models are utilized to warp the slave image, and 20 check points are manually picked from the warped image and the master image to check the registration accuracy. Then AG [32], and LP [30], LS [31] are utilized to perform comparison with the proposed method on the same test dataset.

*1) Line segment matching between high resolution and low resolution image patches:* A pair of Quickbird satellite image patches are utilized in the registration test. Both image patches were acquired in 2004, Nigeria, Africa. One is selected from the multiple spectral image whose spatial resolution is 2.4 meters, and the other is selected from the panchromatic image whose resolution is 0.6 meters. The multiple spectral image patch is the slave one, while the panchromatic image is the master one. For the multiple spectral image patch, the first three bands (blue, green, red) are converted into grayscale [59], and then the grayscale image is utilized to detect line segments. Figure 4 shows the Quickbird satellite image patches and the matched segments using the proposed method.

*2) Line segment matching between ALOS and SPOT-5 image patches:* A pair of remote sensing image patches were utilized in the registration test. One is an unrectified ALOS PRISM 1B2 image patch and the other is an ortho SPOT-5 image patch whose geometric accuracy is better than 5 meters. Both image patches are in Wuhan district of China, and the ALOS image was obtained in 2010 while the SPOT image was obtained in 2004. The ALOS image patch is the slave one, while the ortho SPOT-5 image patch is the master one. Figure 5 shows the ALOS image patch, the SPOT-5 image patch, and the matched line segments using the proposed method.

*3) Line segment matching test between satellite image and GIS layer:* A satellite image patch and a digital map in Ningxia district of China are utilized in this test. The satellite image patch is the slave one, while the digital map is the master one. Figure 6 shows the satellite image patch, the digital map, and the matched line segments using the proposed method.

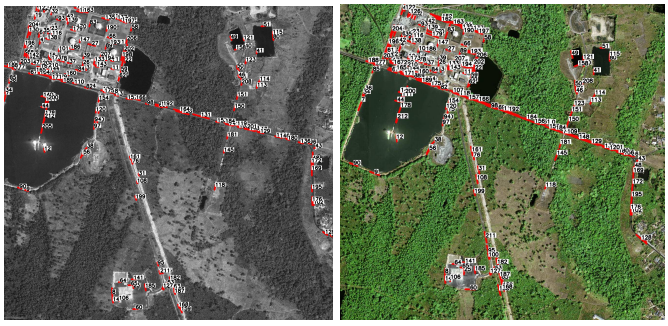

(a) (b)

Fig. 4. Test 1: line segment registration using high resolution and low resolution image patches: (a) The high resolution image patch and the matched line segments. (b) The low resolution image patch and the matched line segments.

From Figure 4, Figure 5 and Figure 6, one can see that not all the pairs of matched line segments are exactly the same in length and position. As a matter of fact, a pair of matched line segments may be different parts of a straight line. And in this sense, a pair of matched line segments actually lies on the corresponding straight lines.

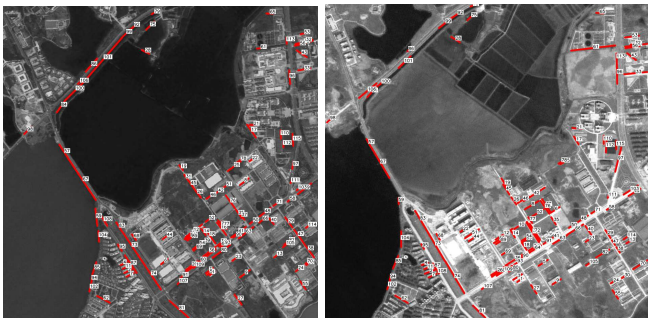

(a) (b)

Fig. 5. Test 2: line segment registration using SPOT-5 and ALOS image patches: (a) The ortho SPOT-5 image patch and the matched line segments. (b) The ALOS PRISM 1B2 image patch and the matched line segments.

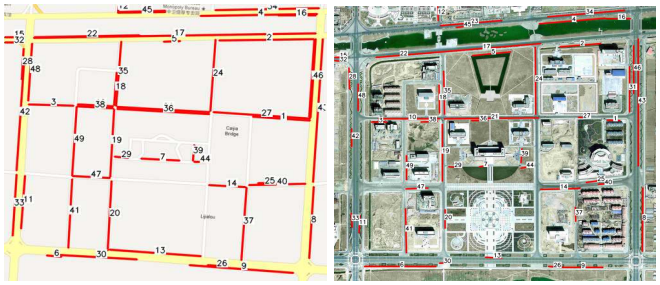

(a) (b)

Fig. 6. Test 3: line segment registration using satellite image and GIS layer: (a) The GIS layer and the matched line segments. (b) The satellite image patch and the matched line segments.

In Figure 4, the image pair are of different spatial resolutions; in Figure 5, the image pair are from different sensors; in Figure 6 the GIS layer is hardly textured. The proposed algorithm successfully found the corresponding line segments from each pair of images.

Our matching results are compared with three other methods, including AG [32], LP [30], and LS [31]. The comparison results are given in Table II. For each image pair, the following results are reported: the number of total matches, the correct ratios and the computational time. Table III shows the sizes of the test image patches.

TABLE III
THE SIZES OF THE TEST IMAGE PATCHES.

| Test Names | Image Size (pixel × pixel) | |
|---|---|---|
| | Master | Slave |
| Test 1 | 2112 × 2012 | 670 × 650 |
| Test 2 | 933 × 913 | 933 × 921 |
| Test 3 | 749 × 806 | 750 × 639 |

According to Table II and Table III, we can see that:

- Although all of the four approaches provide enough line segments to perform a registration for image patches of different spatial resolutions, the other approaches provide significantly less number of matched line segments compared to ours with various correct ratios. Moreover, the results in V-B4 will show that the proposed approach performs a better registration than those of the other approaches.
- LP has a bad matching result for Test 2. As the image patches of Test 2 are quite different in contrast and illumination, repeatable feature points are difficult to extract, and therefore LP which is based on the points correspondences performs poorly.
- The results also show that the proposed method achieves higher matching correctness than other methods. Considering that the proposed method is based on the geometric constraint is over line segments, and that the mismatched line segments are removed in the outlier excluding step, the high matching precision of the proposed method is reasonable.
- In the GIS case, no other than our approach provides correct corresponding line segments. Although sufficient number of line segments is available for matching and registration, the local appearances of line segments are indistinguishable in the GIS layer, and the similarity based matching approaches are infeasible to find correct line segment correspondences.
- It is not surprising that the proposed approach is slower than the descriptor-based approaches when the images are small, because the proposed approach utilizes only the spatial relationship, and its search space is much larger than those of the descriptor-based approaches. However, the computational time of AG, LP and LS is closely related to the sizes of the images, while the case of the proposed approach is quite different. As mentioned in V-A, the number of detected line segments is more likely to affect the the computational time of the proposed approach than the image size. Although AG, LP are much faster when the test images are small, they may be less efficient when the test images are large.

*4) Registration precision:* As the other three matching algorithms (AG [32], LP [30], and LS [31]) do not provide methods to estimate geometric model from control line segments, our estimating method is utilized to perform the registration using the matched line segments of the three algorithms. Additionally, RANSAC approach is utilized to eliminate the outliers in the results of these three methods, and the results of our approach without RANSAC are also provided. The residual errors of the check points of the three tests using eight methods (Our approach without RANSAC, Our approach, AG, AG+RANSAC, LP, LP+RANSAC, LS and LS+RANSAC) are shown in Table IV, and Figure 7 shows the warped image patches (using our approach) and the distribution of the check points.

Following points can be drawn from Table IV and Figure 7:

- According to Figure 7, in Test 1 and Test 3, the check points distribute evenly, but in Test 2, evenly distributed check points are not available due to the great changes between the slave image and master image, and the check points are picked from the unchanged areas. For our approach, Table IV shows that the RMSEs (Root Mean Square Errors) of the check points in Test 1 and Test 2 are within 1 pixel. In Test 3, however, the residual errors

TABLE II
COMPARISON OF OUR APPROACH WITH THREE OTHER LINE SEGMENT MATCHING ALGORITHMS (AG [32], LP [30], AND LS [31]).

| Test Names | Total Matches | | | | Correct Ratios (%) | | | | Time (s) | | | |
|---|---|---|---|---|---|---|---|---|---|---|---|---|
| | Our | AG | LP | LS | Our | AG | LP | LS | Our | AG | LP | LS |
| Test 1 | 212 | 108 | 83 | 64 | 99.5 | 90.7 | 97.6 | 98.4 | 33.998 | 47.757 | 46.815 | 52.042 |
| Test 2 | 115 | 70 | 22 | 60 | 95.7 | 92.9 | 59.1 | 96.7 | 54.198 | 4.739 | 9.897 | 28.913 |
| Test 3 | 49 | 3 | 0 | 8 | 98.0 | 0 | 0 | 0 | 37.045 | 1.849 | 1.510 | 18.918 |

TABLE IV
THE RESIDUAL ERRORS OF THE CHECK POINTS. FOR EACH TEST AND EACH METHOD, THE ROOT MEAN SQUARE ERRORS IN $x$ DIRECTION AND $y$ DIRECTION ARE LISTED IN THE TABLE.

| Methods | Test 1 | | Test 2 | | Test 3 | |
|---|---|---|---|---|---|---|
| | $x$ RMSE (pixel) | $y$ RMSE (pixel) | $x$ RMSE (pixel) | $y$ RMSE (pixel) | $x$ RMSE (pixel) | $y$ RMSE (pixel) |
| Ours-RANSAC | 0.53 | 0.32 | 1.10 | 0.82 | 1.72 | 2.75 |
| Ours | 0.42 | 0.47 | 0.83 | 0.96 | 1.81 | 2.83 |
| AG | 6.73 | 12.91 | 8.90 | 14.29 | — | — |
| AG+RANSAC | 3.58 | 3.52 | 2.47 | 4.33 | — | — |
| LP | 1.50 | 2.84 | — | — | — | — |
| LP+RANSAC | 0.83 | 1.04 | — | — | — | — |
| LS | 1.13 | 2.56 | 3.85 | 4.88 | — | — |
| LS+RANSAC | 0.78 | 1.01 | 2.88 | 3.58 | — | — |

Note: RMSE = Root Mean Square Error, Ours-RANSAC = Ours without RANSAC.

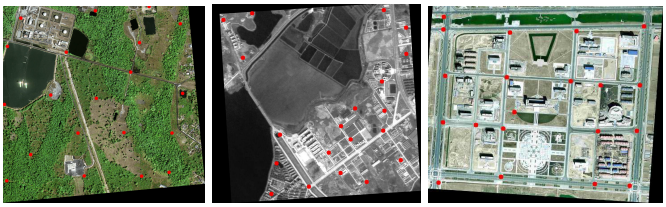

(a) (b) (c)

Fig. 7. The warped image patches and the check points: (a) The warped Quickbird multiple spectral image patch and the distribution of 20 check points. (b) The warped ALOS PRISM 1B2 image patch and the distribution of 20 check points. (c) The warped satellite image patch and the distribution of 20 check points.

of check points are a bit larger.

- According to Table IV, the proposed approach get much better registration precision than others. For the descriptor based matching approaches, some of the estimated geometric models are too incorrect to yield valid warped images, and therefore the RMSEs are noted as null value. As the estimating method for geometric model is sensitive to outliers, those matching results involving a large number of false matchings may not provide satisfied registration results, such as AG in Test 1, AG and LP in Test 2, AG, LP and LS in Test 3. And after eliminating the outliers in the matched line segments, the registration precisions of AG, LP and LS are greatly improved. In contrast, outlier elimination does not evidently improve the registration precisions for our approach. The reason is that the distances of the falsely matched line segment pairs in our approach are commonly not large enough to make the registration too bad.
- As a matter of fact, considering that the line segment features in a vector layer are vectors and do not exactly correspond to the real objects in an image, the registration between a remote sensing image and a GIS vector layer would not be as accurate as that between images. In Figure 6, particularly, the detected line segments in the satellite image may lie on either side of a road, while the line segment feature corresponding to this road in the vector layer is one line, from which one cannot exactly tell where the sides of the road are. Consequently, the registration between images and GIS vector layers may result in inaccuracy due to the uncertainty of the vector data. However, when extra control data are not available, GIS data may be an alternative reference for unrectified remote sensing images.

## VI. CONCLUSIONS AND SUGGESTIONS

This paper has presented a line segment registration method, which does not require the corresponding line segments sharing the same start points and end points. The correspondence and transformation model are simultaneously determined in this method. Instead of considering the line segment descriptors or similarity measures, only the spatial relationship among the line segments is utilized in the proposed method. Test results show that the proposed method is robust to rotation, noise, contrast, brightness and texture. In particular, the less-textured data, such as GIS vector layer involved in the tests, yielded good results, while the registration of such data would be intractable using texture-based similarity measures. Consequently, it is expected to utilize the proposed method to line segment registration between SAR image and optical image. However, the performance of the proposed method can be affected by the quality of the line segments detected. If the detected line segments are fragmented, a large number of short line

segments may make the proposed method computationally expensive. And if the real corresponding line segments in the detected candidates are rare while the outliers are numerous, the proposed method may yield a wrong transformation model, and the line segment correspondences will certainly be fallible. In this sense, a high repeatable line segment detection method will contribute to efficient and robust performance of the line segment registration method, and our future work will be devoted to it. Meanwhile, additional effort should also be made to accelerate the registration algorithm and estimate good initial parameters.

## ACKNOWLEDGEMENTS

The aerial image utilized in this paper is provided by Swiss Federal Office of Topography, and the Quickbird images were downloaded from the website of Satellite Imaging Corporation, and the digital maps were acquired from Baidu Map.

The author is grateful to the anonymous reviewers for carefully reading the manuscript and making useful suggestions.

## REFERENCES

[1] B. Zitova and J. Flusser, "Image registration methods: a survey," *Image and Vision Computing*, vol. 21, no. 11, pp. 977–1000, 2003.

[2] A. Goshtasby, *2-D and 3-D Image Registration: for Medical, Remote Sensing, and Industrial Applications*. Wiley-Interscience, 2005.

[3] D. Lowe, "Object recognition from local scale-invariant features," in *Computer Vision, 1999. The Proceedings of the Seventh IEEE International Conference on*, vol. 2. Ieee, 1999, pp. 1150–1157.

[4] H. Bay, T. Tuytelaars, and L. Van Gool, "Surf: Speeded up robust features," in *European Conference on Computer Vision*, vol. 1. Springer, 2006, pp. 404–417.

[5] E. Tola, V. Lepetit, and P. Fua, "Daisy: An efficient dense descriptor applied to wide-baseline stereo," *IEEE Transactions on Pattern Analysis and Machine Intelligence*, vol. 32, no. 5, pp. 815–830, 2010.

[6] S. Leutenegger, M. Chli, and R. Siegwart, "Brisk: Binary robust invariant scalable keypoints," in *Computer Vision (ICCV), 2011 IEEE International Conference on*. IEEE, 2011, pp. 2548–2555.

[7] E. Rublee, V. Rabaud, K. Konolige, and G. Bradski, "Orb: an efficient alternative to sift or surf," in *Computer Vision (ICCV), 2011 IEEE International Conference on*. IEEE, 2011, pp. 2564–2571.

[8] A. Alahi, R. Ortiz, and P. Vandergheynst, "Freak: Fast retina keypoint," in *Computer Vision and Pattern Recognition (CVPR), 2012 IEEE Conference on*. IEEE, 2012, pp. 510–517.

[9] A. Habib, R. Al-Ruzouq, and C. Kim, "Semi-automatic registration and change detection using multi-source imagery with varying geometric and radiometric properties," *Photogrammetric Engineering & Remote Sensing*, vol. 71, no. 3, pp. 325–332, 2005.

[10] P. David, D. DeMenthon, R. Duraiswami, and H. Samet, "Simultaneous pose and correspondence determination using line features," in *Computer Vision and Pattern Recognition, 2003. Proceedings. 2003 IEEE Computer Society Conference on*, vol. 2. IEEE, 2003, pp. II–424.

[11] A. Habib, M. Morgan, E. Kim, and R. Cheng, "Linear features in photogrammetric activities," *International Archives of Photogrammetry and Remote Sensing*, vol. 35, pp. 610–615, 2004.

[12] L. Quackenbush, "A review of techniques for extracting linear features from imagery," *Photogrammetric Engineering & Remote Sensing*, vol. 70, no. 12, pp. 1383–1392, 2004.

[13] R. Hartley, "Projective reconstruction from line correspondences," in *Computer Vision and Pattern Recognition, 1994. Proceedings CVPR'94., 1994 IEEE Computer Society Conference on*. IEEE, 1994, pp. 903–907.

[14] L. Quan and T. Kanade, "Affine structure from line correspondences with uncalibrated affine cameras," *IEEE Transactions on Pattern Analysis and Machine Intelligence*, vol. 19, no. 8, pp. 834–845, 1997.

[15] T. Schenk, "From point-based to feature-based aerial triangulation," *ISPRS Journal of Photogrammetry and Remote Sensing*, vol. 58, no. 5, pp. 315–329, 2004.

[16] W. Shi and A. Shaker, "The line-based transformation model (lbtm) for image-to-image registration of high-resolution satellite image data," *International Journal of Remote Sensing*, vol. 27, no. 14, pp. 3001–3012, 2006.

[17] A. Tommaselli and C. Tozzi, "A recursive approach to space resection using straight lines," *Photogrammetric Engineering & Remote Sensing*, vol. 62, no. 1, pp. 57–65, 1996.

[18] F. Van den Heuvel, "A line-photogrammetric mathematical model for the reconstruction of polyhedral objects," in *Proceedings of SPIE*, vol. 3641. San Jose CA, USA, 1999, pp. 60–71.

[19] Z. Zhang and J. Zhang, "Generalized point photogrammetry and its application," in *The 20th ISPRS Congress, Commission*, vol. 5, 2004, pp. 77–81.

[20] Z. Zhang, Y. Zhang, J. Zhang, and H. Zhang, "Photogrammetric modeling of linear features with generalized point photogrammetry," *Photogrammetric Engineering & Remote Sensing*, vol. 74, no. 9, pp. 1119–1127, 2008.

[21] T. Teo, "Line-based rational function model for high-resolution satellite imagery," *International Journal of Remote Sensing*, vol. 34, no. 4, pp. 1355–1372, 2013.

[22] Z. Liu and R. Marlet, "Virtual line descriptor and semi-local graph matching method for reliable feature correspondence," in *Proceedings of the British Machine Vision Conference*. BMVA Press, 2012, pp. 16.1–16.11.

[23] S. Mosaddegh, D. Fofi, and P. Vasseur, "Short base-line line matching for central imaging systems," *Pattern Recognition Letters*, vol. 33, no. 16, pp. 2292–2301, 2012.

[24] A. Ok, J. Wegner, C. Heipke, F. Rottensteiner, U. Soergel, and V. Toprak, "Matching of straight line segments from aerial stereo images of urban areas," *ISPRS Journal of Photogrammetry and Remote Sensing*, vol. 74, pp. 133–152, 2012.

[25] C. Schmid and A. Zisserman, "Automatic line matching across views," in *Computer Vision and Pattern Recognition, 1997. Proceedings., 1997 IEEE Computer Society Conference on*. IEEE, 1997, pp. 666–671.

[26] H. Liu, Z. Wang, and C. Deng, "Extend point descriptors for line, curve and region matching," in *Machine Learning and Cybernetics (ICMLC), 2010 International Conference on*, vol. 1. IEEE, 2010, pp. 214–219.

[27] Z. Wang, F. Wu, and Z. Hu, "Msld: A robust descriptor for line matching," *Pattern Recognition*, vol. 42, no. 5, pp. 941–953, 2009.

[28] M. Zouqi, J. Samarabandu, and Y. Zhou, "Multi-modal image registration using line features and mutual information," in *Image Processing (ICIP), 2010 17th IEEE International Conference on*. IEEE, 2010, pp. 129–132.

[29] C. Zhang and E. P. Baltsavias, "Edge matching and 3d road reconstruction using knowledge-based methods," in *Institute of Geodesy and Photogrammetry, ETH H. onggerberg, CH-8093*, 2000.

[30] B. Fan, F. Wu, and Z. Hu, "Line matching leveraged by point correspondences," in *Computer Vision and Pattern Recognition (CVPR), 2010 IEEE Conference on*. IEEE, 2010, pp. 390–397.

[31] L. Wang, U. Neumann, and S. You, "Wide-baseline image matching using line signatures," in *Computer Vision, 2009 IEEE 12th International Conference on*. IEEE, 2009, pp. 1311–1318.

[32] L. Zhang and R. Koch, "Line matching using appearance similarities and geometric constraints," *Pattern Recognition*, pp. 236–245, 2012.

[33] A. Habib, D. Kelley, and A. Asmamaw, "New approach to solving matching problems in photogrammetry," *International Archives of Photogrammetry and Remote Sensing*, vol. 33, no. B2; PART 2, pp. 257–264, 2000.

[34] G. Danchao, T. Xiaotao, L. Shizhong, and H. Guojun, "Image registration of high resolution remote sensing based on straight line feature," in *International Society for Photogrammetric and Remote Sensing Symposium*, 2008, pp. 1819–1823.

[35] A. Habib, M. Ghanma, M. Morgan, and R. Al-Ruzouq, "Photogrammetric and lidar data registration using linear features," *Photogrammetric Engineering & Remote Sensing*, vol. 71, no. 6, pp. 699–707, 2005.

[36] A. Habib, H. Lin, and M. Morgan, "Line-based modified iterated hough transform for autonomous single-photo resection," *Photogrammetric Engineering & Remote Sensing*, vol. 69, no. 12, pp. 1351–1358, 2003.

[37] S. Shin, A. Habib, M. Ghanma, C. Kim, and E. Kim, "Algorithms for multi-sensor and multi-primitive photogrammetric triangulation," *ETRI journal*, vol. 29, no. 4, pp. 411–420, 2007.

[38] D. Klinec, "A model based approach for orientation in urban environments," in *Proceedings of the XXth Congress of the ISPRS*, vol. 35, 2004, pp. 903–908.

[39] R. P. Horaud, F. Forbes, M. Yguel, G. Dewaele, and J. Zhang, "Rigid and articulated point registration with expectation conditional maximization," *IEEE Transactions on Pattern Analysis and Machine Intelligence*, vol. 33, no. 3, pp. 587 –602, March 2011.

[40] B. Jian and B. C. Vemuri, "A robust algorithm for point set registration using mixture of gaussians." in *10th IEEE International Conference on Computer Vision (ICCV 2005), 17-20 October 2005, Beijing, China*, 2005, pp. 1246–1251.

[41] S. Rusinkiewicz and M. Levoy, "Efficient variants of the icp algorithm," in *3-D Digital Imaging and Modeling, 2001. Proceedings. Third International Conference on*. IEEE, 2001, pp. 145–152.

[42] Z. Zhang, "Iterative point matching for registration of free-form curves and surfaces," *International Journal of Computer Vision*, vol. 13, no. 2, pp. 119–152, 1994.

[43] H. Chui and A. Rangarajan, "A new point matching algorithm for non-rigid registration," *Computer Vision and Image Understanding*, vol. 89, no. 2, pp. 114–141, 2003.

[44] A. Rangarajan, H. Chui, and F. Bookstein, "The softassign procrustes matching algorithm," in *Information Processing in Medical Imaging*. Springer, 1997, pp. 29–42.

[45] H. Chui and A. Rangarajan, "A feature registration framework using mixture models," in *Mathematical Methods in Biomedical Image Analysis, 2000. Proceedings. IEEE Workshop on*. IEEE, 2000, pp. 190–197.

[46] B. Jian and B. Vemuri, "A robust algorithm for point set registration using mixture of gaussians," in *Computer Vision, 2005. ICCV 2005. Tenth IEEE International Conference on*, vol. 2. IEEE, 2005, pp. 1246–1251.

[47] B. Jian and B. C. Vemuri, "Robust point set registration using gaussian mixture models," *IEEE Transactions on Pattern Analysis and Machine Intelligence*, vol. 33, no. 8, pp. 1633–1645, 2011.

[48] A. Myronenko and X. Song, "Point set registration: Coherent point drift," *IEEE Transactions on Pattern Analysis and Machine Intelligence*, vol. 32, no. 12, pp. 2262–2275, 2010.

[49] D. Reynolds, T. Quatieri, and R. Dunn, "Speaker verification using adapted gaussian mixture models," *Digital Signal Processing*, vol. 10, no. 1, pp. 19–41, 2000.

[50] A. Dempster, N. Laird, and D. Rubin, "Maximum likelihood from incomplete data via the em algorithm," *Journal of the Royal Statistical Society. Series B (Methodological)*, pp. 1–38, 1977.

[51] K. Krishnamoorthy, *Handbook of statistical distributions with applications*. Chapman & Hall/CRC, 2006, vol. 188.

[52] K. Ni, H. Jin, and F. Dellaert, "Groupsac: Efficient consensus in the presence of groupings," in *Computer Vision, 2009 IEEE 12th International Conference on*. IEEE, 2009, pp. 2193–2200.

[53] T. Long, W. Jiao, and W. Wang, "Geometric rectification using feature points supplied by straight-lines," *Procedia Environmental Sciences*, vol. 11, pp. 200–207, 2011.

[54] M. Lourakis, "levmar: Levenberg-marquardt nonlinear least squares algorithms in C/C++," http://www.ics.forth.gr/ lourakis/levmar/, Jul. 2004, (Accessed on 31 Jan. 2005.).

[55] C. Fraser and T. Yamakawa, "Insights into the affine model for high-resolution satellite sensor orientation," *ISPRS Journal of Photogrammetry and Remote Sensing*, vol. 58, no. 5, pp. 275–288, 2004.

[56] C. Fraser and H. Hanley, "Bias compensation in rational functions for ikonos satellite imagery," *Photogrammetric Engineering & Remote Sensing*, vol. 69, no. 1, pp. 53–57, 2003.

[57] R. Von Gioi, J. Jakubowicz, J. Morel, and G. Randall, "Lsd: A fast line segment detector with a false detection control," *IEEE Transactions on Pattern Analysis and Machine Intelligence*, vol. 32, no. 4, pp. 722–732, 2010.

[58] P. J. Besl and N. D. McKay, "A method for registration 3-d shapes," *IEEE Transactions on Pattern Analysis and Machine Intelligence*, vol. 14, no. 2, pp. 239–256, 1992.

[59] M. Stokes, M. Anderson, S. Chandrasekar, and R. Motta, "A standard default color space for the internet-srgb," *Microsoft and Hewlett-Packard Joint Report*, 1996.


**Tengfei Long** was born in Wuhan, P. R. China, in 1986. He received the B.Sc. degree in remote sensing from Wuhan University, in 2008. And he received the M.Sc. degree in cartography and geographic information systems from Center for Earth Observation and Digital Earth, Chinese Academy of Sciences (CAS), Beijing, China, in 2011.

In 2011, he joined the Insititute of Remote Sensing and Digital Earth, CAS, as a research assistant. Since September 2013, he has been a Ph.D candidate in the Insititute of Remote Sensing and Digital Earth, Chinese Academy of Sciences. His current research interests include spatial photogrammetry, image registration, land-cover change detection and computer vision.

**Weili Jiao** received the B.Sc. in cartography from Wuhan University, China, in 1988 and the M.Sc. in Geoinformatics from ITC, the Netherland, in 1995.

Since 2001, she has been an Associate Professor at Institute of Remote Sensing and Digital Earth (RADI), formerly known as Center for Earth Observation and Digital Earth (2007-2012), and China Remote Sensing Satellite Ground Station (before 2007), Chinese Academy of Sciences. She was an Assistant Professor at China Remote Sensing Satellite Ground Station from 1988 to 2001. Her current research interests include digital photogrammetry, image registration, image feature extraction, land-cover mapping and change detection.

**Guojin He** was born in Fujian province, P. R. China, in 1968. He received the B.Sc. in geology from Fuzhou University in 1989 and the M.Sc. in remote sensing of geology from China University of Geosciences (Wuhan), in 1992. And he got the Ph.D. in geology from Institute of Geology, Chinese Academy of Sciences (CAS), in 1998.

From 1992 to 2007, he worked at the Information Processing Department of China Remote Sensing Satellite Ground Station (RSGS), CAS. In 2001, He became the deputy director of Information Processing Department of RSGS, CAS. From 2004, he was the Professor and director of Information Processing Department of RSGS, and also headed the research group of Remote Sensing Information Mining and Intelligent Processing. From 2008-2012, he was the professor and director of the Value-added Product Department, and the deputy director of the Spatial Data Center, Center for Earth Observation and Digital Earth, CAS. Since 2013, he has been the professor and director of the Satellite Data Based Value-added Product Department, and the deputy director of RSGS, Institute of Remote Sensing and Digital Earth, CAS. A large part of his earlier research dealt with information processing and applications of satellite remote sensing data. His current research interests are focusing on optical high resolution remote sensing image understanding as well as using information retrieved from satellite remote sensing images, in combination with other sources of data to support better understanding of the earth.

**Wei Wang** received the B.Sc. in earth sciences from Zhejiang University, China, in 1997.

In 1997, he joined the China Remote Sensing Satellite Ground Station, Chinese Academy of Sciences (CAS). Since 2009, he has been a senior engineer at Institute of Remote Sensing and Digital Earth (RADI), formerly known as Center for Earth Observation and Digital Earth (2007-2012), and China Remote Sensing Satellite Ground Station (before 2007), CAS. His current research interests include geometrical data processing for remotely sensed data and image registration.